JOURNAL OF GUIDANCE, CONTROL, AND DYNAMICS
Vol. 16, No. 6, November–December 1993

H_2 Optimal Halo Orbit Guidance

Brian L. Jones* and Robert H. Bishop†
University of Texas at Austin, Austin, Texas 78712

An output feedback guidance law for a halo orbit about the translunar equilibrium point in the circular restricted three-body problem is developed. The equations of motion are derived and the location and stability of the translunar equilibrium point discussed. The halo orbit guidance problem is formulated in the frequency domain from which an output feedback guidance law is developed using H_2 control theory. Simulation results validate the guidance law and provide data that quantify the effect of control inputs, noise characteristics, and halo orbit characteristics on the steady-state halo orbit stationkeeping costs.

Introduction

HALO orbits were primarily investigated in the late 1960s when NASA began examining follow-on lunar exploration opportunities to the Apollo program. In an effort to open up the far side of the moon to exploration, studies were undertaken to determine if continuous communications or staging operations with a far side lunar base could be accomplished. More recently, a NASA report[1] investigated four approaches to a manned mission to Mars. Common to all four approaches was the deployment of a telecommunications satellite in translunar halo orbit to support far side lunar communications. Figure 1 shows the geometry of the translunar halo orbit. The translunar equilibrium point is inherently unstable and chaotic; active guidance will be required to maintain the halo orbit.

Many investigators have examined the general halo orbit guidance problem; this paper will summarize only those sources that directly apply to the translunar halo orbit guidance problem. Farquhar[2,3] and Farquhar and Kamel[4] provided an extensive review of previous work done on controlling an orbit about an equilibrium point. They considered controlling a halo orbit about the translunar equilibrium point and showed that using a simple proportional plus derivative controller provided asymptotic stability while minimizing the control acceleration required. Deviations from the desired orbit were not considered in the minimization. Breakwell et al.[5] formulated the halo orbit guidance problem as a periodic system. They used the classical optimal control approach with the addition of an observer to the system model. Position deviations were considered in their problem formulation, but only results for a large halo orbit radius were given.

Subsequently, a flight dynamics study[6] of both the halo and hummingbird concepts was completed; the hummingbird concept places a spacecraft at a stationary offset position from the equilibrium point. Both concepts were found to be feasible, but the halo orbit was preferred because it has fewer propulsion requirements for stationkeeping. This study's problem formulation used a frequency matching guidance law with discrete impulses applied twice an orbit. Heppenheimer[7] used phase-plane methods to construct a family of locally fuel-optimal out-of-plane period controls. Vonbun[8] also investigated using a hummingbird orbit rather than a halo orbit and found in general that it required 10% more acceleration to maintain the desired position. More recently, Fraietta and Bond[9] computed stationkeeping costs for halo orbits about both the cislunar and translunar equilibrium points.

Finally, Farquhar[10] compared the use of a polar lunar orbit and a halo orbit for lunar exploration staging operations. He concluded that a halo orbit space station could offer important operational and performance advantages compared with a polar lunar orbit station. Among these advantages were increased communication opportunities with the lunar surface and increased launch windows for transfers between the space station and the lunar surface.

This research takes a different approach by using H_2 control theory to formulate the halo orbit guidance problem as a continuous thrust system in the frequency domain. The advantage to the frequency domain problem formulation is that it can be extended to modern control theories, such as H_2 and H_∞ theory, so that the class of plant disturbances and measurement noises considered can be expanded. This paper presents a guidance law that stabilizes the translunar halo orbit and minimizes the position deviation from the halo orbit plus the control acceleration. The relevant equations of motion are given in the next section. Subsequently, the system models, guidance law computation, and simulation results are presented. Finally, the last section summarizes this research and draws general conclusions.

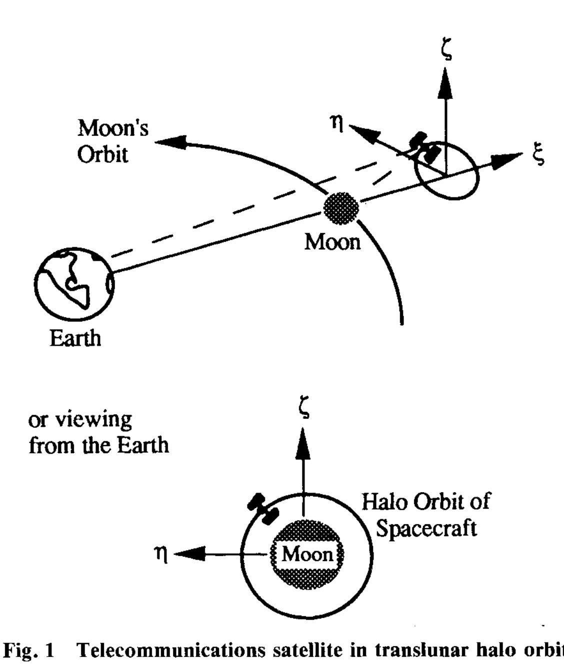

Fig. 1 Telecommunications satellite in translunar halo orbit.

Received May 18, 1992; presented as Paper 92-4658 at the AIAA/AAS Astrodynamics Conference, Hilton Head, SC, Aug. 10–12, 1992; revision received March 8, 1993; accepted for publication March 16, 1993.

*Graduate Student, Department of Aerospace Engineering and Engineering Mechanics; Major, U.S.A.F. Senior Member AIAA.

†Assistant Professor, Department of Aerospace Engineering and Engineering Mechanics. Senior Member AIAA.

Table 1 Equilibrium point locations

Equilibrium point	x	y
Translunar, L_1	1.155682	0
Cislunar, L_2	0.836915	0
Trans-Earth, L_3	−1.005063	0
Triangular, $L_{4,5}$	0.487849	±0.866025

Circular Restricted Problem of Three Bodies

Investigation into the problem of three bodies dates back to the 18th century. In 1772, Lagrange showed the existence of equilibrium points in the restricted three-body problem. This problem has been the focus of much research in classical celestial mechanics; Szebehely[11] devoted an entire volume to just this subject. The circular restricted three-body problem defines a system where two primary bodies revolve around their barycenter in circular orbits under the influence of their mutual gravitational attraction, and the third body, which has significantly less mass, is attracted by the two primary bodies but does not influence their motion. The circular restricted problem of three bodies mathematically describes the motion of the third body.

Nonlinear Equations of Motion

The derivation of the nondimensional equations of motion for the circular restricted three-body problem is well known (see Szebehely,[11] for example). The halo orbit guidance problem adds one additional term in each equation, U, corresponding to the control acceleration on the spacecraft. Hence,

$$\ddot{x} - 2\dot{y} - x = -\left\{\frac{\mu[x-(1-\mu)]}{\rho_{MS}^3} + \frac{(1-\mu)[x+\mu]}{\rho_{ES}^3}\right\} + U_x \quad (1)$$

$$\ddot{y} + 2\dot{x} - y = -y\left\{\frac{\mu}{\rho_{MS}^3} + \frac{(1-\mu)}{\rho_{ES}^3}\right\} + U_y \quad (2)$$

$$\ddot{z} = -z\left\{\frac{\mu}{\rho_{MS}^3} + \frac{(1-\mu)}{\rho_{ES}^3}\right\} + U_z \quad (3)$$

where

$$\rho_{MS} = \sqrt{[x-(1-\mu)]^2 + y^2 + z^2} \quad (4)$$

$$\rho_{ES} = \sqrt{[x+\mu]^2 + y^2 + z^2} \quad (5)$$

and where x, y, and z are the nondimensional position components of the spacecraft in each axis of the rotating coordinate system, and μ is the mass ratio of the two primary bodies.

Equilibrium points occur when all external forces are balanced. Assuming no active propulsion by the spacecraft, Eqs. (1-3) produce the equilibrium points given in Table 1 for the Earth-moon system ($\mu = 0.01215057$)[12]; the z component is identically equal to zero for each point. Figure 2 shows the geometry of these points.

Linearized Equations of Motion

Equations (1-3) can be written in functional matrix form as

$$\dot{X} = f[X(t)] + g[U(t)] \quad (6)$$

where

$$X \triangleq [x\ y\ z\ \dot{x}\ \dot{y}\ \dot{z}]^T \quad \text{and} \quad U \triangleq [U_x\ U_y\ U_z]^T \quad (7)$$

Define the linearized state and control as

$$\boldsymbol{\Omega} \triangleq [\xi\ \eta\ \zeta\ \dot{\xi}\ \dot{\eta}\ \dot{\zeta}]^T \triangleq X - X_{\text{nom}} \quad \text{and} \quad \boldsymbol{u} \triangleq U - U_{\text{nom}} \quad (8)$$

where $(\ )_{\text{nom}}$ denotes a nominal value. Neglecting the higher order terms in a Taylor series expansion yields

$$\dot{\boldsymbol{\Omega}} = \boldsymbol{A}_G\boldsymbol{\Omega} + \boldsymbol{B}_G\boldsymbol{u} \quad (9)$$

where

$$\boldsymbol{A}_G = \left[\frac{\partial f}{\partial X}\right]_{\text{nom}} \quad \text{and} \quad \boldsymbol{B}_G = \left[\frac{\partial g}{\partial U}\right]_{\text{nom}} \quad (10)$$

Consider a nominal halo orbit of small radius centered about an equilibrium point. The guidance law can then be developed about the stationary equilibrium point and the nominal halo orbit added to the closed-loop system as a perturbation; a halo orbit radius of 3500 km has a maximum perturbation of 0.8%. Treating the nominal halo orbit in this manner allows the linearized equations of motion to become time invariant rather than periodic. For the translunar equilibrium point,

$$\boldsymbol{A}_G = \begin{bmatrix} \boldsymbol{0} & \boldsymbol{I} \\ \boldsymbol{A}_{G21} & \boldsymbol{A}_{G22} \end{bmatrix} \quad \text{and} \quad \boldsymbol{B}_G = \begin{bmatrix} \boldsymbol{0} \\ \boldsymbol{I} \end{bmatrix} \quad (11)$$

where

$$\boldsymbol{A}_{G21} = \begin{bmatrix} 7.380861 & 0 & 0 \\ 0 & -2.190431 & 0 \\ 0 & 0 & -3.190431 \end{bmatrix} \quad (12)$$

and

$$\boldsymbol{A}_{G22} = \begin{bmatrix} 0 & 2 & 0 \\ -2 & 0 & 0 \\ 0 & 0 & 0 \end{bmatrix} \quad (13)$$

Note the ζ axis can be uncoupled from the ξ and η axes after the linearization.

Periodic Orbits

The unforced solution to Eq. (9) can be solved analytically:

$$\xi(t) = C_1\exp(-\tau t) + C_2\exp(\tau t) + C_3\cos(\omega_1 t) + C_4\sin(\omega_1 t) \quad (14)$$

$$\eta(t) = C_5\exp(-\tau t) + C_6\exp(\tau t) + C_7\cos(\omega_1 t) + C_8\sin(\omega_1 t) \quad (15)$$

$$\zeta(t) = C_9\cos(\omega_2 t) + C_{10}\sin(\omega_2 t) \quad (16)$$

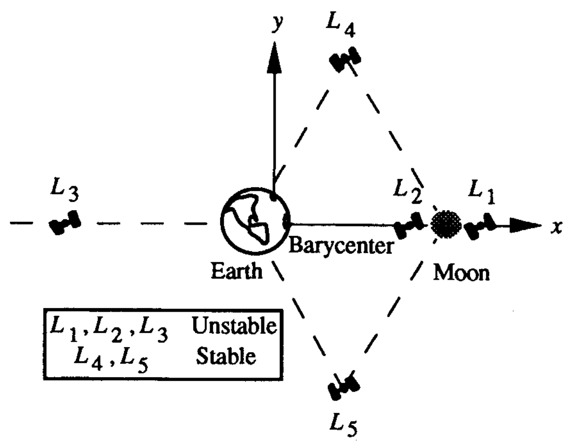

Fig. 2 Equilibrium point locations.

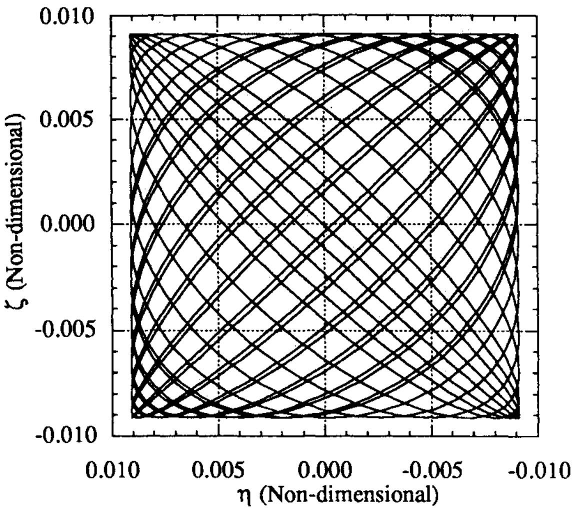

Fig. 3 Uncontrolled periodic orbit.

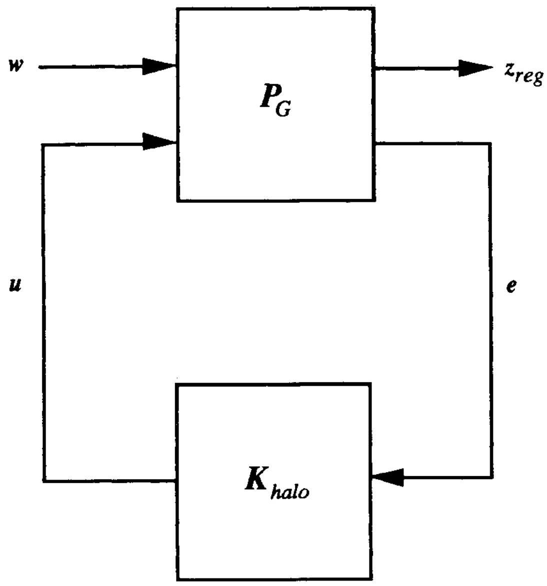

Fig. 4 H_2 system model.

where

$$\tau = 2.158677, \quad \omega_1 = 1.862647, \quad \omega_2 = 1.786178 \tag{17}$$

and C_1–C_{10} are constants of integration and functions of the initial position and velocity of the spacecraft. In general, Eqs. (14–16) are unbounded; thus, the linear system is unstable. However, if the initial conditions are chosen properly, the exponential terms can be eliminated. In addition, if the periodic orbit is chosen to be centered about L_1, that is, $\xi(0) = 0$, and the initial point of the orbit is selected so that $\dot{\zeta}(0) = 0$, Eqs. (14–16) further reduce to

$$\xi(t) = 0.343334\eta(0)\sin(1.862647t) \tag{18}$$

$$\eta(t) = \eta(0)\cos(1.862647t) \tag{19}$$

$$\zeta(t) = \zeta(0)\cos(1.786178t) \tag{20}$$

It is readily apparent that a small radius halo orbit, that is, the region where the linear system is valid, cannot exist without active guidance because of the different natural frequencies between the η axis and the ζ axis. Figure 3 graphically illustrates this result by choosing $\eta(0)$ and $\zeta(0)$ to be 0.00911 (3500 km) and 90 deg out-of-phase. This Lissajous trajectory clearly shows periods of time when the moon will block the line-of-sight between the Earth and a spacecraft; this period of blockage equates to a disk with a radius of 0.00806 (3100 km) centered at the origin on Fig. 3.

Halo Orbit Guidance Law

H_2 control theory minimizes the two norm of the closed-loop transfer function T_{zw}, between the regulated variables z_{reg} and the exogenous inputs w; the H_2 system model is shown in Fig. 4. A precise problem statement is as follows:

$$\text{Minimize } \|T_{zw}\|_2 \tag{21}$$

where the regulated variables are chosen to be

$$z_{\text{reg}} = [\rho_\eta \eta \quad \rho_\zeta \zeta \quad u^T]^T \tag{22}$$

and the exogenous inputs are chosen to be

$$w = [w_d^T \quad w_m^T]^T \tag{23}$$

The plant disturbances w_d and the measurement noise w_m have a fixed power spectrum. In addition, ρ_η and ρ_ζ are selectable constants so that the relative weighting of position deviation and control acceleration can be varied. Since the deviation in the ξ axis does not affect the line-of-sight between the halo orbit and Earth, ξ was not included as a regulated variable.

System Models

Desired System Model

Figure 5 shows the desired system model where G represents the plant and K_{halo} represents the guidance law. The plant and guidance law have the general realizations

$$G = \left[\begin{array}{c|c} A_G & B_G \\ \hline C_G & D_G \end{array}\right] \quad \text{and} \quad K_{\text{halo}} = \left[\begin{array}{c|c} A_K & B_K \\ \hline C_K & D_K \end{array}\right] \tag{24}$$

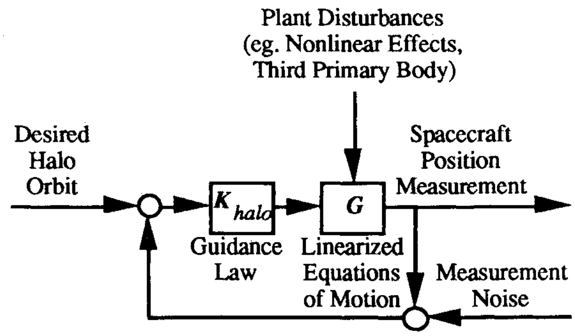

Fig. 5 Desired system model.

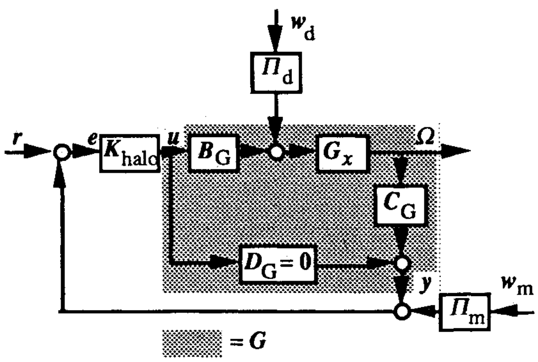

Fig. 6 Expanded system model.

Figure 6 shows an expanded system model where G has been broken down into its realization parts; G_x has the realization

$$G_x = \left[\begin{array}{c|c} A_G & I \\ \hline I & 0 \end{array}\right] \tag{25}$$

In this paper, only position measurements are considered. Hence,

$$C_G = [I \quad 0] \qquad \text{and} \qquad D_G = 0 \tag{26}$$

The environment consists of plant disturbances and measurement noise, both modeled as white Gaussian noise with zero mean and identity covariance. The plant disturbance, or process noise, is then scaled by a nondimensional matrix Π_d,

$$\Pi_d = \begin{bmatrix} \pi_v I & 0 \\ 0 & \pi_a I \end{bmatrix} \tag{27}$$

where π_v and π_a are the nondimensional square root of the fixed power spectrum in velocity and acceleration, respectively. The measurement noise has also been scaled by a nondimensional matrix Π_m,

$$\Pi_m = \pi_p I \tag{28}$$

where π_p is the nondimensional square root of the fixed power spectrum in position.

H_2 System Model

Figure 4 shows the system model required by Doyle et al.[13] for the two Riccati equation H_2 control system design method. The plant P_G in this system model has the general realization

$$P_G = \left[\begin{array}{c|cc} A & B_1 & B_2 \\ \hline C_1 & D_{11} & D_{12} \\ C_2 & D_{21} & D_{22} \end{array}\right] \tag{29}$$

and requires a particular structure for the D matrices. Dailey[14] summarized a method for loop shifting and scaling these matrices; this method uses the singular value decomposition of the D_{12} and D_{21} matrices to transform a general system model into the desired form. Transforming the expanded system model (Fig. 6) into the H_2 system model and applying scaling yields

$$\tilde{P}_G = \left[\begin{array}{c|cc:c} A_G & \Pi_d & 0 & B_G \\ \hline \rho_\eta \alpha_\eta & 0 & 0 & 0 \\ \rho_\zeta \alpha_\zeta & 0 & 0 & 0 \\ 0 & 0 & 0 & I \\ \hdashline \Pi_m^{-1} C_G & 0 & I & 0 \end{array}\right] \tag{30}$$

where ($\tilde{\ }$) indicates scaled parameters and α_η and α_ζ are matrices defined such that

$$\eta = \alpha_\eta \Omega \qquad \text{and} \qquad \zeta = \alpha_\zeta \Omega \tag{31}$$

State-Space H_2 Solution

The H_2 optimal solution involves solving two algebraic Riccati equations.[13] The first Riccati equation (X_2) represents state feedback; the second Riccati equation (Y_2) represents observer feedback. For this system, the two Riccati equations are

$$X_2 A_G - X_2 B_G B_G^T X_2 + A_G^T X_2 + \rho_\eta^2 \alpha_\eta^T \alpha_\eta + \rho_\zeta^2 \alpha_\zeta^T \alpha_\zeta = 0 \tag{32}$$

$$Y_2 A_G^T - Y_2 C_G^T \Pi_m^{-T} \Pi_m^{-1} C_G Y_2 + A_G Y_2 + \Pi_d \Pi_d^T = 0 \tag{33}$$

Table 2 Simulation noise statistics

	Fixed power spectrum	Average state σ
Position	$\pi_p^2 = 2.665$ m^2/s	9.637 km
Velocity	$\pi_v^2 = 2.665e-8$ m^2/s^3	1.152 m/s
Acceleration	$\pi_a^2 = 1.666e-15$ m^2/s^5	N/A

Table 3 ΔV_{TOT} comparison

Study	ΔV_{TOT}, m/s/day
Midrange weighting	0.2997
Minimum weighting	0.1549
Farquhar[3]	0.2839
Flight dynamics[6]	0.2800
Heppenheimer[7]	0.2929
Fraietta and Bond[9]	0.7934

Given the solutions to Eqs. (32) and (33), the feedback gain matrix becomes

$$F_2 = -B_G^T X_2 \tag{34}$$

and the observer gain matrix is

$$L_2 = -Y_2 C_G^T \Pi_m^{-T} \Pi_m^{-1} \tag{35}$$

Finally, the optimum guidance law is given by

$$K_{\mathrm{halo}} = \left[\begin{array}{c|c} A_{\tilde{K}} & B_{\tilde{K}} \Pi_m^{-1} \\ \hline C_{\tilde{K}} & 0 \end{array}\right] \tag{36}$$

where

$$A_{\tilde{K}} = A - B_G B_G^T X_2 - Y_2 C_G^T \Pi_m^{-T} \Pi_m^{-1} C_G \tag{37}$$

$$B_{\tilde{K}} = Y_2 C_G^T \Pi_m^{-T} \tag{38}$$

$$C_{\tilde{K}} = -B_G^T X_2 \tag{39}$$

Simulation Results

A simulation was developed to validate the guidance law given in Eq. (36). For the initial cases examined, linear simulation results were found to be in agreement with nonlinear simulation results. Therefore, the linear simulation was used to generate the results presented in this paper. Data from two typical H_2 optimal guidance laws are given first, followed by three parametric studies.

Typical H_2 Guidance Law

The simulation was run for 300 days (20 revolutions of the halo orbit) using midrange weighting parameters ($\rho_\eta = 170$ and $\rho_\zeta = 550$) and minimum control acceleration weighting parameters ($\rho_\eta = 36$ and $\rho_\zeta = 1000$). The noise statistics used in the simulations are given in Table 2. These statistics are consistent with the tracking accuracy study contained in the flight dynamics study.[6] The variations in the average total steady-state propulsion requirement per day (ΔV_{TOT}) with respect to these input parameters are discussed in detail in Jones[15] and summarized in the next section. The reference input was a clockwise circular halo orbit with a radius of 3500 km and a nondimensional frequency of 1.862647.

The resultant system states and the control accelerations are sinusoidal functions at the selected halo orbit frequency. The estimation error is quickly driven to zero by the observer in all states. Table 3 compares these typical guidance laws with previous results; these results do not include process or measurement noise.

A robustness analysis was done for the guidance law using midrange weighting parameters. Structured uncertainty was used to represent error sources such as neglected high-frequency dynamics, input actuator errors, and low-frequency plant parameter errors. As expected, the gain and phase margins were reduced with the addition of the observer into the guidance law. The gain and phase margin could be improved through the loop transfer recovery technique; however, this procedure was not applied to this guidance law.

Figure 7 gives the geometric view of the halo orbit for the midrange weighting parameters H_2 optimum guidance law when both process noise and measurement noise are absent from the simulation; Fig. 8 applies when 3σ process noise and 3σ measurement noise are included. The orbits are stable and repeatable, and the line-of-sight with the Earth is never lost. When noise is included in the simulation, the deviations from the desired halo orbit are small.

Control Input Parametric Study

Three-axis vs two-axis control (ξ and ζ axes) was investigated to determined the advantages or disadvantages of each method. The figures-of-merit for this parametric study were chosen to be the average steady-state ΔV per day for maintaining the orbit (ξ and η axes) and the percent steady-state error from the desired circular halo orbit.

Table 4 gives the results for three cases (a–c) where the semiminor axis steady-state error of the resultant halo orbit was held constant; the position weighting factors were varied to maintain constant semiminor axis errors. Semiminor axis errors more negative than -11.43% indicate a loss of line-of-sight with the Earth. In addition, the average steady-state ΔV per day in the ζ axis was held constant. Three-axis control

Table 4 Three- vs two-axis control

Control axes		ΔV_ξ	ΔV_η	Major	Minor
		m/s/day		% error	
(a)	3	7.866	2.694	4.85	−11.55
	2	0.034	—	11.92	−11.34
(b)	3	8.124	2.778	4.20	−5.42
	2	0.063	—	8.53	−5.26
(c)	3	8.476	2.890	2.62	−0.94
	2	0.209	—	4.03	−0.95

Table 5 ξ vs η axis control

Control axes		ΔV_ξ	ΔV_η	Major	Minor
		m/s/day		% error	
(a)	ξ	0.034	—	11.92	−11.34
	η	—	0.034	65.84	−27.62
(b)	ξ	0.063	—	8.53	−5.26
	η	—	0.063	47.29	−78.86
(c)	ξ	0.209	—	4.03	−0.95
	η	—	0.209	42.12	−91.56

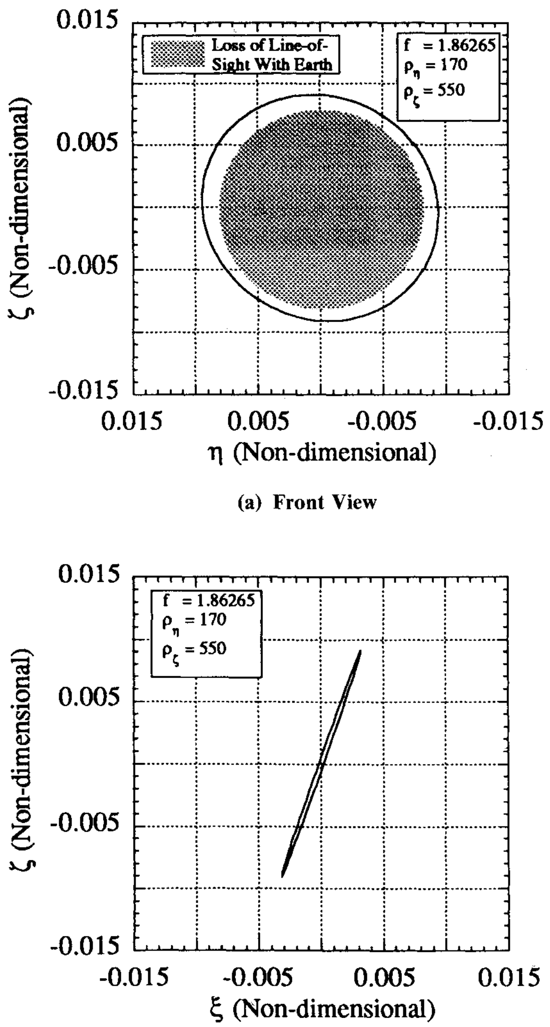

(a) Front View

(b) Side View

Fig. 7 Halo orbit geometry (zero noise).

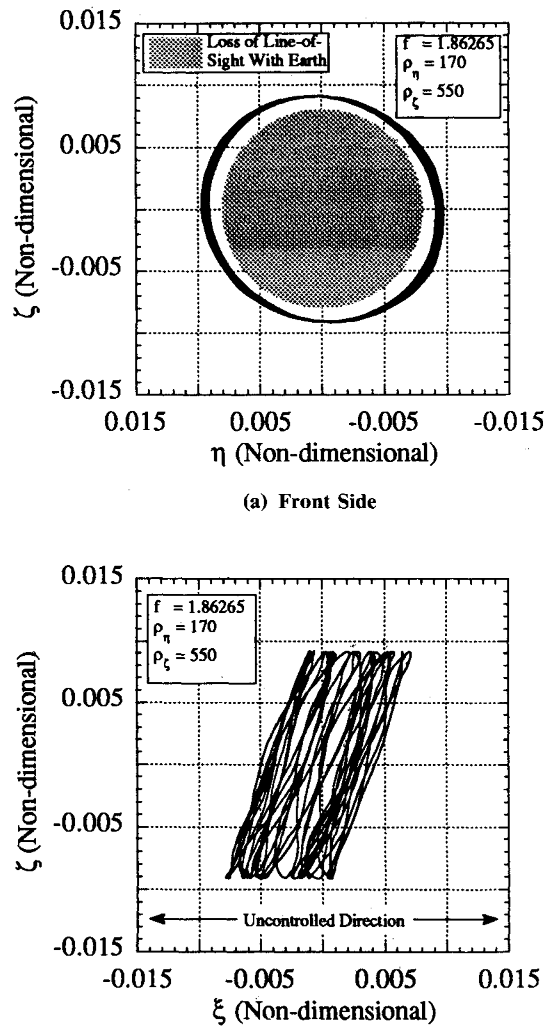

(a) Front Side

(b) Side View

Fig. 8 Halo orbit geometry (3σ noise).

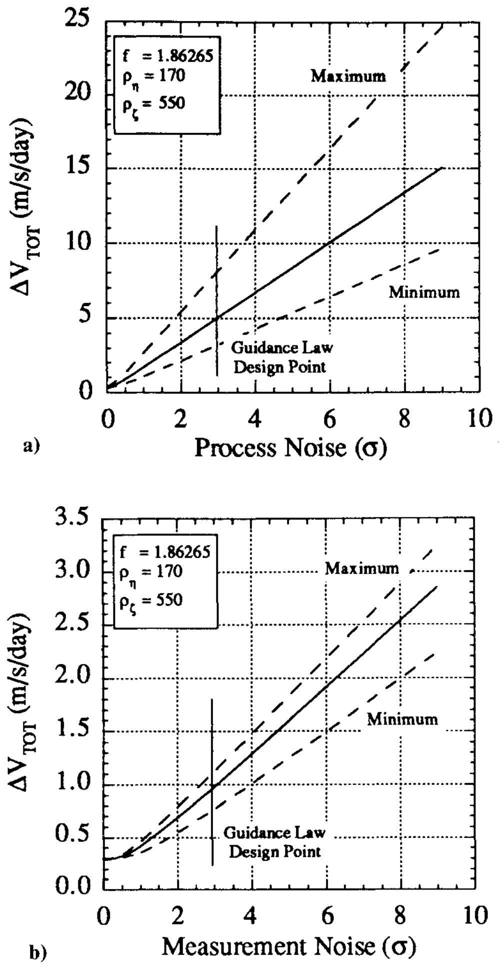

Fig. 9 Effect of noise on halo orbit stationkeeping cost.

provided a better resultant halo orbit that was closer to the desired circular orbit. However, the ΔV associated with the tighter control was two orders of magnitude higher.

Two-axis control, using either control in the ξ or η axis, was also investigated for advantages or disadvantages. Table 5 gives the results for three cases (a–c) where the average steady-state ΔV per day for each case was held constant; the position weighting factors were varied to maintain constant average steady-state ΔV per day. Two-axis control using the ξ axis provided much tighter resultant halo orbits for the same propulsion cost. Hence, two-axis control using the ξ and ζ axes is used in the remaining simulations.

Noise Characteristics Parametric Study

The steady-state solution to the observer Riccati equation is the error covariance associated with the estimated system states. Equation (33) shows that the error covariance is a function of $\mathbf{\Pi}_d$ and $\mathbf{\Pi}_m$. The noise statistics used in the simulations are given in Table 2. These statistics are consistent with the tracking accuracy study contained in the flight dynamics study.[6] A Monte Carlo analysis was completed to quantify the effect of these noise statistics on the average steady-state ΔV per day for halo orbit maintenance. Thirty 150-day simulations were run and the resultant average steady-state ΔV per day obtained. In all cases, the reference input to the simulation was a clockwise circular halo orbit with a radius of 3500 km and a nondimensional frequency of 1.862647. Midrange weighting parameters were also used. Figure 9 shows essentially a linear relationship between the amount of process noise and measurement noise and the resultant average steady-state ΔV per day. The dashed lines show the minimum and maximum values obtained in the 30 simulations. The average steady-state ΔV per day found in Table 3 corresponds to zero process noise and zero measurement noise.

Halo Orbit Characteristics Parametric Study

The position weighting factors ρ_η and ρ_ζ and the halo orbit frequency were varied to determine the effects of each. Nondimensional frequency was varied from 0.2 to 7.4 for each case. As before, the reference input to the simulation was a clockwise circular halo orbit with a radius of 3500 km. The duration of each simulation was 150 days.

In each case, the resultant steady-state halo orbit was an ellipse. For halo orbits with clockwise orbital rotation, Fig. 10 shows, qualitatively, the effect on the halo orbit of increasing the desired halo orbit frequency. The minimum deviation from a purely vertical orientation was obtained at a nondimensional frequency of 1.47. As the halo orbit's nondimensional frequency deviated from the system's natural frequency (1.862647), velocity requirements in both axes increased rapidly. When the nondimensional frequency was reduced by 1, the average steady-state ΔV per day increased by a factor of 30. For an increase in the nondimensional frequency of 1, the average steady-state ΔV per day increased by a factor of 50.

The halo orbit nondimensional frequency was then fixed at the natural frequency of the system, and the position weighting factors were varied. The geometry of the halo orbit was essentially constant with respect to changes in the ζ axis weighting

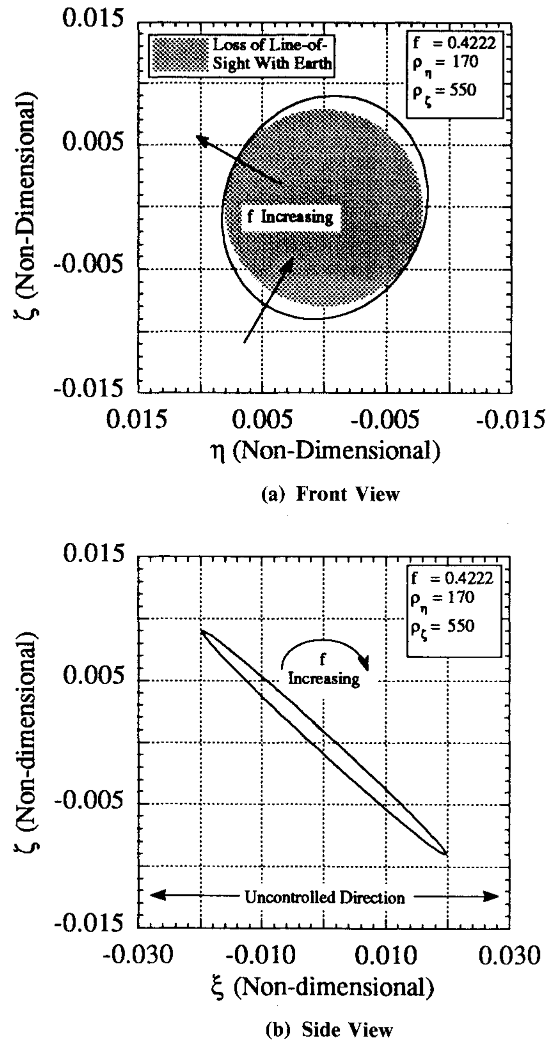

Fig. 10 Effect of increasing frequency on halo orbits with clockwise orbital rotation.

factor, and the steady-state error decreased as the η axis weighting factor increased. The orientation of the halo orbit was essentially constant for changes in either weighting factor. Because of the uncoupling of the linearized equations of motion, the velocity required in the ξ axis was only influenced by the weighting factor in the η axis; the velocity required increased as the weighting factor increased. Similarly, the velocity required in the ζ axis was only influenced by the weighting factor in the ζ axis. However, in this case, the velocity required decreased as the weighting factor increased. This was due to the ζ axis originally being stable and the coupled ξ and η axes having to be stabilized by the guidance law.

Conclusions

A guidance law has been developed using H_2 control theory that stabilizes the translunar halo orbit in the restricted three-body problem. This guidance law minimizes the position deviation from the desired halo orbit plus the control acceleration. Simulation results validated the guidance law. Furthermore, the halo orbit guidance problem has been formulated in the frequency domain. Other frequency domain design techniques, such as H_∞ control theory, are now directly applicable. Finally, the effects of halo orbit frequency, position weighting factor, and the amount of process noise or measurement noise present have been quantified.

Acknowledgment

Support for the graduate studies of the first author has been provided by the United States Air Force. This source of support is gratefully acknowledged.

References

[1] "Report of the 90-Day Study on Human Exploration of the Moon and Mars," NASA, Nov. 1989.

[2] Farquhar, R. W., "The Control and Use of Libration-Point Satellites," NASA-TR-R-346, Sept. 1970.

[3] Farquhar, R. W., "The Utilization of Halo Orbits in Advanced Lunar Operations'," NASA-TN-D-6365, July 1971.

[4] Farquhar, R. W., and Kamel, A. A., "Quasi-Periodic Orbits About the Translunar Libration Point," *Celestial Mechanics,* Vol. 7, No. 4, 1973, pp. 458–473.

[5] Breakwell, J. V., Kamel, A. A., and Ratner, M. J., "Station-Keeping for a Translunar Communication Station," *Celestial Mechanics,* Vol. 10, No. 3, 1974, pp. 357–373.

[6] Porter, J. D., "Final Report for Lunar Libration Point Flight Dynamics Study," NASA CR-130135, April 1969.

[7] Heppenheimer, T. A., "Optimal Controls for Out-of-Plane Motion about the Translunar Libration Point," *Journal of Spacecraft and Rockets,* Vol. 7, No. 9, 1970, pp. 1087–1092.

[8] Vonbun, F. O., "A Hummingbird for the L_2 Lunar Libration Point," NASA TN-D-4468, April 1968.

[9] Fraietta, M. F., and Bond, V. R., "Libration Point Stationkeeping in the Earth-Moon System," McDonnell Douglas Space System Co., TM-3.50.01-09, Houston, TX, June 1991; see also "Station Keeping near the Unstable Libration Points of the Restricted Three-Body Problem," NASA JSC-24597, Oct. 1990.

[10] Farquhar, R. W., "A Halo-Orbit Lunar Station," *Astronautics and Aeronautics,* Vol. 10, No. 6, 1972, pp. 59–63.

[11] Szebehely, V., *Theory of Orbits: The Restricted Problem of Three Bodies,* Academic Press, New York, 1967.

[12] *The Astronomical Almanac,* U.S. Government Printing Office, Washington, DC, 1991.

[13] Doyle, J. C., Glover, K., Khargonekar, P. P., and Francis, B. A., "State-Space Solutions to Standard H_2 and H_∞ Control Problem," *IEEE Transactions on Automatic Control,* Vol. 34, No. 8, 1989, pp. 831–847.

[14] Dailey, R. L., "Lecture Notes for the Workshop on H_∞ and μ Methods for Robust Control," 1990 American Control Conference, San Diego, CA, May 1990.

[15] Jones, B. L., "Spacecraft Rendezvous for the Restricted Three-Body Problem, Dissertation Progress Report," Center for Controls and Systems Research Rept. 1001-92, University of Texas at Austin, Austin, TX, April 1992.